Received: 24 January 2024 | Revised: 29 May 2024 | Accepted: 13 July 2024

DOI: 10.1002/aic.18549

AIChE JOURNAL

RESEARCH ARTICLE

Process Systems Engineering

Modeling and simulation of bi-continuous jammed emulsion membrane reactors for enhanced biphasic enzymatic reactions

Aref Ghoreishee[1] | Daeyeon Lee[2] | Dimitrios Papavassiliou[3] | Kathleen Stebe[2] | Masoud Soroush[1]

[1]Department of Chemical and Biological Engineering, Drexel University, Philadelphia, Pennsylvania, USA

[2]Department of Chemical and Bimolecular Engineering, University of Pennsylvania, Philadelphia, Pennsylvania, USA

[3]School of Sustainable Chemical Biological and Materials Engineering, University of Oklahoma, Norman, Oklahoma, USA

Correspondence
Masoud Soroush, Department of Chemical and Biological Engineering, Drexel University, Philadelphia, PA 19104, USA.
Email: ms1@drexel.edu

Funding information
National Science Foundation, Grant/Award Number: CBET-2132141

Abstract

Bi-continuous jammed emulsion (bijel) membrane reactors, integrating simultaneous reaction and separation, offer a promising avenue for enhancing membrane reactor processes. In this study, we present a comprehensive macroscopic-scale physico-chemical model for tubular bijel membrane reactors and a numerical solution strategy for solving the governing partial differential equations. The model captures the co-continuous network of two immiscible phases stabilized by nanoparticles at the liquid–liquid interface. We present the derivation of model equations and an efficient numerical solution strategy. The model is validated with experimental results from a conventional enzymatic biphasic membrane reactor for oleuropein hydrolysis, already reported in the literature. Simulation results indicate accurate prediction of reactor behavior, highlighting the potential superiority of bijel membrane reactors over current technologies. This research contributes a valuable tool for scale-up, design, and optimization of bijel membrane reactors, filling a critical gap in this emerging field.

KEYWORDS
bijel membrane, biphasic membrane reactor, enzymatic bioconversion, process intensification

1 | INTRODUCTION

Membrane reactors have shown immense potential in chemical industries, because they allow for the simultaneous occurrence of reactions and separation in one single unit. The use of such technology usually leads to consumption of less energy and to a smaller processing unit.[1] An application of these reactors is in enzymatic bioconversion, in which raw materials are converted to valuable products, or toxic materials are decomposed into benign compounds. As such, they have been used in the pharmaceutical, food, and waste treatment industries.[2] The idea of performing enzymatic-based reactions in membrane reactors has been extensively studied and also has been successfully translated to commercial processes.[3–6] The basic idea in these reactors is the immobilization of enzymes in the sponge layer of the membrane where there is a large area for the enzymatic reactions. Studies have shown that the immobilization can enhance the enzyme activity.[2,3,7,8]

An enzyme membrane reactor can be monophasic or biphasic. In a monophasic enzyme reactor, both reactants and products are either in an aqueous or in an oily phase, while the membrane provides a zone for reactions to occur and acts as a filter. In fact, in a monophasic enzyme reactor, as the substrate passes through the membrane, both diffusion and convective flow occurs in the reaction zone, leading to effective product removal and improved reactor performance.[9] Product removal from the reaction area, especially in the cases where product inhibition can occur, is crucial. On the other hand, in a biphasic enzyme membrane reactor, reactants and products are not in the same phase. Aqueous and oily phases flow in the shell and lumen sides of the membrane. These two immiscible streams deliver reactants to and remove products from the spongy layer of the membrane. These reactors have been used in applications such as esterification and hydrolysis.[10–12] In conventional biphasic membrane reactors, based on the hydrophilic or hydrophobic properties of the

membrane matrix, a hydrophilic-hydrophobic interface is formed, and entire enzymes are immobilized in this region known as the enzymatic gel layer.[3] Although the enzyme immobilization does not affect the enzyme activity, in biphasic membrane reactors enzyme activity decreases with increased gel layer thickness because of a rise in the diffusion resistance and the deformation of the molecular structure.[3] When the reaction kinetics involve product inhibition, the reactant conversion decreases because of the diffusion resistance in the enzyme gel layer. For example, in reference 4 it was shown that in a membrane reactor, by increasing the residence time the reaction rate initially increases and then decreases.

Bi-continuous interfacially jammed emulsion gel (bijel) membrane reactors can be used to address the problem of thick enzymatic gel layers. Bijel is a medium consisting of two immiscible liquids (typically an oily and an aqueous phase) that are stabilized by a layer of particles or surfactants at the interface between them. In fact, bijels provide a robust micro-interface for forming a co-continuous network of two immiscible phases throughout the material. Because of these characteristics, bijels are good reaction media for biphasic reactions. A recent experimental study of a bijel membrane as a membrane reactor for biphasic enzymatic reactions showed promising results.[13] The basic idea is to use a bijel as the reacting media instead of the sponge layer of a hollow fiber membrane, allowing the membrane to act as a mechanical support for the bijel. An enzyme is immobilized on the surface of particles, creating an interface between two immiscible phases. Two co-continuous flow networks of reactants and products in the oily and aqueous phases are formed throughout the bijel. This approach alleviates the problems of product inhibition and loss of enzyme activity that occur in conventional membrane reactors, leading to a higher conversion. Furthermore, the bijel provides a larger interfacial area per unit volume in comparison to a conventional membrane matrix for biphasic reactions. Despite their promising characteristics, bijel membrane reactors are in the initial stages of development. Two major challenges are the feasibility and reliability of bijel fabrication. Recent efforts to address these challenges include the fabrication of bijel membranes via solvent transfer-induced separation.[14–19]

While the area of mathematical modeling of monophasic and biphasic membrane reactors is mature,[20,21] little attention has been given to the mathematical modeling of bijel membrane reactors. Comprehensive mathematical models including momentum, heat transfer, and mass transfer and interfacial thermodynamic equilibrium equations for different types of membranes have been presented.[20,21] The momentum equations for single-phase membrane reactors can be simplified to the Darcy equation, which makes the overall mathematical model more computationally tractable. For biphasic membrane reactors, in which two miscible phases flow within a membrane, in general mathematical models should account for two-phase flow in porous media.[22,23]

Nagy et al.[9] used a mathematical model for single-phase flow in a porous medium to describe a conventional membrane reactor with a biphasic reaction, and validated the model with experimental data reported in reference 4. However, due to the presence of both aqueous and oily phases in the membrane voids of a biphasic conventional membrane reactor, a more complex model that accounts for saturation and capillary pressure was needed.[23] Furthermore, Nagy et al.[9] assumed that the reaction product is removed from the reaction sites instantaneously; the reaction rate is not decreased by product inhibition. As at high residence times there is no aqueous flow within the membrane, instantaneous removal of the product from reaction sites is unlikely. This assumption of no product inhibition led to poor accuracy of the reported model at high residence time. As their results show, in the case of a highly hydrophobic or highly hydrophilic membrane, a single-phase flow model can predict the behavior of the biphasic membrane with good accuracy. As in a bijel membrane reactor the oily and aqueous phases flow in separate and connected intertwined channel, models of single-phase flow in porous media can be used to model bijel membrane reactors.

In this work, we present a macroscopic-scale mathematical model for tubular bijel reactors. As the model involves coupled partial differential equations that are difficult to solve with available commercial software products, a solution strategy for solving coupled partial differential equations in cylindrical coordinates is proposed. This strategy is based on the control volume approach presented for the cartesian coordinates in reference 24. We also address the issue of the low accuracy of the upwind strategy for solving coupled partial differential equations involving velocity terms in cylindrical coordinates. In view of the increasing interest in process intensification in many industries including pharmaceutical, food, and water treatment, bijel membrane reactors have the potential to revolutionize the conventional biphasic membrane reactors and thus contribute to process intensification. Considering this potential and the application of process models in the process scale-up, design, and optimization, this study of the mathematical modeling of bijel membrane reactors is timely.

The focus of this work is on the development and validation of a physicochemical process model of a class of bijel membrane reactors. Section 2 describes various parts of a bijel membrane reactor and the derivation of the mathematical model and appropriate boundary conditions. Section 3 proposes a numerical solution strategy to solve the model equations. Section 4 considers a case study and evaluates the predictions of the developed model. Section 5 uses the model to gain insights into the effect of different design parameters and operating parameters on the performance of the reactor. Finally, Section 6 provides some concluding remarks.

2 | PROCESS DESCRIPTION

Pickering emulsions have shown immense potential for biphasic reactions.[25–27] They provide a biphasic medium for reaction and separation. However, reaction and separation in a continuous manner is not possible in these systems, because the delivery of reactants to and the removal of products from reaction sites cannot be achieved simultaneously.[15] Bijels can be considered as a type of Pickering emulsions, but unlike Pickering emulsions that have continuous and

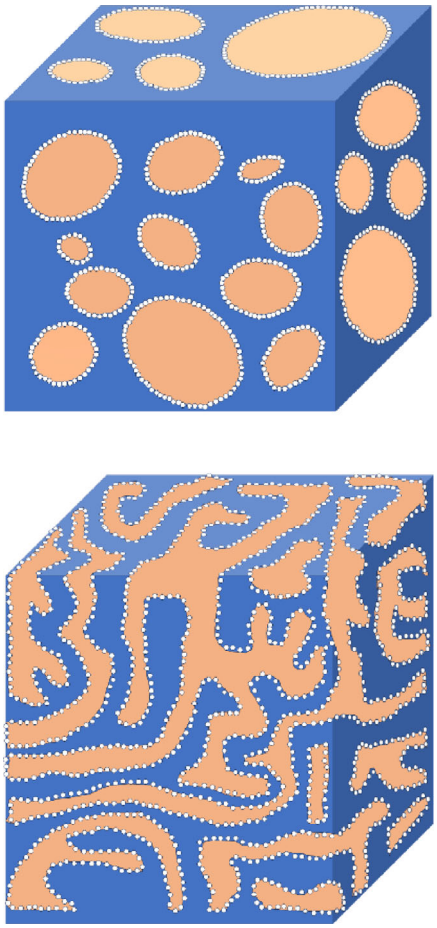

FIGURE 1 A conventional Pickering emulsions biphasic system (top) versus a bijel system (bottom).

isolated phases, they contain co-continuous phases. In recent years, the feasibility and reliability of bijel manufacturing have been studied.[16,17,19] A bijel is a structure that contains co-continuous subregions of oily and aqueous phases throughout the medium. In other words, a bijel can be considered as a porous medium containing oily and aqueous phases in separate intertwined microchannels. Figure 1 depicts a schematic of the structure of a bijel and a Pickering emulsion system.

A promising structure design is to coat a membrane surface by a bijel,[28] so that the membrane acts as a support for the bijel as reactions occur inside the bijel. Figure 2 shows a schematic of a bijel membrane reactor that uses this structure. It should be noted that a bijel can be used as a membrane reactor without a conventional membrane support too. However, a membrane support increases the mechanical stability of the structure.[28]

Although experimental studies demonstrated that bijel membrane reactors with enzymatic biphasic reactions outperform conventional membrane reactors with the same,[28] no study on the mathematical modeling of the former reactors has been reported.

To derive a macroscopic-scale mathematical model of the bijel reactor shown in Figure 2, we divide the reactor into the following four regions (see also Figure 2):

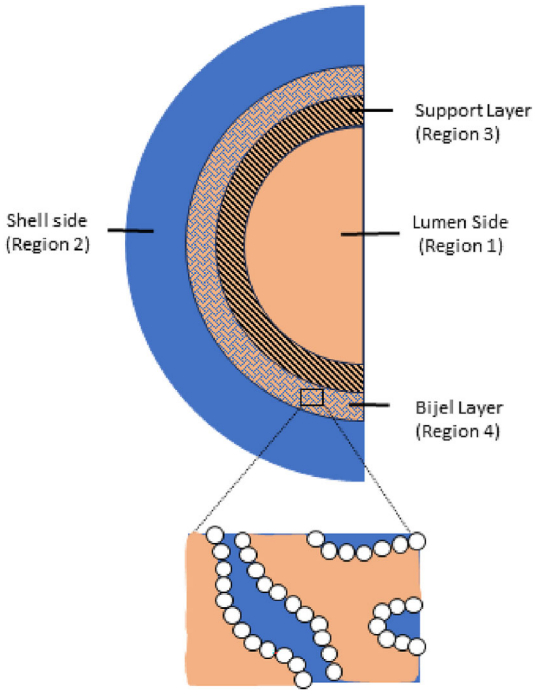

FIGURE 2 Schematic of a bijel membrane reactor.[28]

- Region 1: lumen side;
- Region 2: shell side;
- Region 3: support layer (porous membrane);
- Region 4: bijel layer.

For the four regions, assuming Newtonian incompressible fluids, laminar flows, and isothermal conditions, total mass, momentum, and component mass balances lead to[29]:

$$\nabla.\vec{v} = 0, \tag{1}$$

$$\rho\frac{D\vec{v}}{Dt} = -\nabla p + \mu\nabla^2\vec{v} + \rho\vec{g}, \tag{2}$$

$$\frac{Dc_i}{Dt} = D_i\nabla^2 c_i + \mathcal{R}_i, \tag{3}$$

where $\frac{D}{Dt}$ and ∇ denote the material derivative and gradient operator, respectively. $\rho, \vec{v}, p,$ and μ represent the fluid density, velocity, pressure, and viscosity, respectively. c_i is the concentration of component i.

2.1 | Mathematical modeling of the lumen and shell sides

Based on the geometrical and physical features of the system, by using the same approach as in references 9, 20, 30, further

simplifications can be made. Because the channel diameters are small (in the range of 0.2 – 1.0 mm) and the fluid velocities are low (in the range of 1 – 300 mm/s), Reynolds numbers are very low (0.5 – 100).[9] Thus, inertia-related terms in the momentum equation can be ignored. Based on the hydraulic permeability of bijel[19] and conventional hollow fiber membranes, the traverse velocity should be in the order of 10^{-4} to 10^{-7} m/s, and the axial velocity in the order of 10^{-3} to 10^{-1} m/s.[9] Given the external and internal radii and the length of a typical conventional membrane, it can be concluded that the Peclet number in the axial direction is on the order of 10^4, and in the radial direction in the order of 10^{-3}.[20] As a result, in the axial direction of the lumen and shell sides flow, diffusion-related terms can be ignored, and in the radial direction, mass-transfer convective-related terms can be ignored. Furthermore, we assume steady state conditions. Based on these assumptions and the absence of reactions in these two regions, the definition of the material derivative, and the continuity equation (Equation (1)), Equations (2) and (3) simplify to:

$$\frac{1}{r}\frac{\partial}{\partial r}\left(rv_r^l\right)+\frac{\partial v_z^l}{\partial z}=0, \tag{4}$$

$$\frac{\partial P^l}{\partial r}=0\Rightarrow P^l=P^l(z), \tag{5}$$

$$\frac{\partial P^l}{\partial z}=\mu^l\left(\frac{\partial^2 v_z^l}{\partial r^2}+\frac{1}{r}\frac{\partial v_z^l}{\partial r}\right), \tag{6}$$

$$\frac{\partial\left(v_z^l c_i^l\right)}{\partial z}=D_i^l\left(\frac{\partial^2 c_i^l}{\partial r^2}+\frac{1}{r}\frac{\partial c_i^l}{\partial r}\right), \tag{7}$$

where v_r^l and v_z^l are the radial and axial components of the velocity and l denotes lumen or shell sides.

2.2 | Mathematical modeling of the bijel layer

As discussed in Section 2.1, a bijel can be considered as two separate co-continuous phases throughout the medium as shown in Figure 1. In other words, from the aqueous or oily phase viewpoint, the bijel can be modeled as a reacting single-phase flow in a porous medium. It has been assumed that no swelling occurs in the bijel structure due to the diffusion and reaction, the aqueous and oily fractions are constant, and the phases are continuous throughout the region. Like flow in a porous medium, superficial and intrinsic velocities can be defined for each phase, and these two velocities are related to each other according to:

$$\vec{u}^{\,l}=\varepsilon^l\vec{U}^{\,l}, \tag{8}$$

where u^l and U^l denote superficial and intrinsic velocities of phase l (aqueous or oily), respectively, and ε^l is the volume fraction of phase l of the bijel. Using Equation (8) and applying the same approach for mathematical modeling of membrane matrices in reference 21 to this case, Equations (1)–(3) become:

$$\frac{\partial\left(\varepsilon^l\rho^l\right)}{\partial t}+\nabla.\left(\varepsilon^l\rho^l\vec{U}^{\,l}\right)=0, \tag{9}$$

$$\frac{\partial\left(\varepsilon^l\rho^l\vec{U}^{\,l}\right)}{\partial t}+\nabla.\left(\varepsilon^l\rho^l\vec{U}^{\,l}\vec{U}^{\,l}\right)=-\nabla p+\mu^l\nabla^2\left(\varepsilon^l\vec{U}^{\,l}\right)+\varepsilon^l\rho^l\vec{g}-\varepsilon^l\vec{F}, \tag{10}$$

$$\frac{\partial\left(c_i^l\right)}{\partial t}+\nabla.\left(\varepsilon^l c_i^l\vec{U}^{\,l}\right)=D_i^l\nabla^2\left(c_i^l\right)+\mathcal{R}_i, \tag{11}$$

where $\vec{F}$ represents additional momentum losses due to the flow in intertwining microchannels in the medium and is defined as follows[31]:

$$\vec{F}=\bar{f}_1\vec{U}^{\,l}+\bar{f}_2\vec{U}^{\,l}\left|\vec{U}^{\,l}\right|, \tag{12}$$

where $\bar{f}_1$ and $\bar{f}_2$ are model parameters and can be calculated analytically and/or experimentally.[31] $\mathcal{R}_i$ is the rate of consumption or generation of component i. Equations (9)–(11) describe the bijel under constant temperature assumption. D_i^l is the diffusivity of component i in the bijel, which is calculated using[3]:

$$D_i^l=\frac{D_i\varepsilon^l}{\tau^l}, \tag{13}$$

where τ^l is the tortuosity of the bijel with respect to phase l, and D_i is the diffusivity of component i in the solution.

The bijel structure is complex, as it involves the transport of two co-continuous phases in separate intertwining regions. Although Equations (9)–(11) provide a comprehensive description of the bijel, their solution is computationally demanding. Also, $\vec{F}$, which is an extension of Darcy's law (Equation 12), contains empirical coefficients, which add to the uncertainty of the model. Thus, further simplification can be made.

Based on the work presented in reference 19, the bijel can be considered as an isotropic porous medium with a definite permeability for each phase. As a result, by applying Darcy's law and the steady-state assumption, the following simpler equations are obtained:

$$\vec{u}^{\,l}=-\frac{K^l}{\mu^l}\nabla p, \tag{14}$$

$$\frac{\partial^2 P}{\partial r^2}+\frac{1}{r}\frac{\partial P}{\partial r}+\frac{\partial^2 P}{\partial z^2}=0, \tag{15}$$

$$\frac{1}{r}\frac{\partial}{\partial r}\left(ru_r^l c_i\right)+\frac{\partial}{\partial z}\left(u_z^l c_i\right)=D_i^l\left(\frac{\partial^2 c_i}{\partial r^2}+\frac{1}{r}\frac{\partial c_i}{\partial r}+\frac{\partial^2 c_i}{\partial z^2}\right)+\mathcal{R}_i, \tag{16}$$

where K^l is the permeability of phase l in the bijel.

2.2.1 | Reaction kinetics

Many of the enzymatic reactions can be modeled based on the Michaelis–Menten kinetics model.[32] In many cases, the kinetics model should contain product inhibition terms to represent realistic cases.[33] Product inhibition has a negative effect on the conversion of the reactants, and as the concentrations of the products increase (higher conversion), the negative effect increases. In the case of biphasic reactions, it can be assumed that an unstable biphasic equilibrium layer forms around the enzymes, and the reactant and product concentrations in this layer are proportional to their concentrations in bulk phases.[32] In conventional membrane reactors, a sponge layer of immobilized enzymes with two-phase flow forms, and the concentration of products in the sponge layer affects the reaction conversion. Experimental studies showed that as the residence time increases, the conversion in a membrane reactor increases and reaches a plateau (in which any further increase in the residence time does not increase the conversion).[4] However, in a bijel membrane reactor, because two immiscible phases have separate channels for co-continuous flow, and enzymes are usually immobilized on the surface of particles that makes the interface between two immiscible phases, the products can freely flow from the reaction site.[13] As a result, less product inhibition occurs in the bijel, leading to a higher conversion at the plateau. Thus, it is reasonable to assume that equations representing enzymatic reactions in a bijel system should not contain the product inhibition term. Figure 1 depicts the difference between a conventional biphasic system and a bijel system.

Here, we use the Michaelis–Menten kinetics model:

$$\mathcal{R}_i = \frac{\mathcal{R}_m c}{k_m + c + \frac{k_m}{k_I} c_p}, \tag{17}$$

where $\mathcal{R}_m$ and k_m are Michelis-Menten parameters, k_m is a function of the total specific interfacial area for the reaction,[34] and k_I is the inhibition coefficient. Consequently, based on the described structures, it is expected that k_m be lower for bijel membrane reactors than for membrane reactors. Furthermore, k_I is infinite for bijel membrane reactors, while it is finite for conventional membrane reactors. $\mathcal{R}_m$ is the maximum value of the reaction rate and is proportional to the active enzyme concentration.[34] The solid matrix which is available for the enzyme immobilization in the bijel is formed from many spherical jammed nanoparticles. The importance of this is twofold—higher surface area for enzyme immobilization and more importantly higher oil–water interface area. While it is true that the surface area per se is not particularly high, a bijel allows for increasing the interfacial area (from 2D to 3D). Thus, bijels provide a higher surface area in comparison to the solid matrix of conventional membranes. Furthermore, in a bijel, the enzyme can be immobilized on both sides of the nanoparticles (oily and aqueous sides). A quantitative microstructural comparison of bijels revealed that bijel benefits from uniform pore-size distributions for both oily and aqueous domains, which results in attractive transport pathways in both oily and aqueous domains.[35] As a result, bijels are expected to have a larger active surface area for enzyme immobilization and reaction, in comparison to the conventional membrane matrix for biphasic reactions. Furthermore, in a bijel, a microstructural analysis of the bijel on the other hand, bijels show a more continuous and engineered surface area in comparison to conventional porous media.[36] Consequently, it is expected that the value of $\mathcal{R}_m$ be higher for a bijel membrane reactor than for a conventional membrane reactor.

2.3 | Mathematical modeling of the support layer

As mentioned earlier, the support layer (porous membrane) acts as a mechanical support in the bijel membrane reactor. As can be seen in Figure 2, in a bijel membrane reactor, the porous membrane contains a single phase in which no reaction occurs. However, the porous membrane can be eliminated from the structure, if the bijel itself has sufficient mechanical strength.[15] As a result, the same equations in (14)–(16) can be applied to this region, but the reaction term should be set to zero.

2.4 | Interface of regions

As mentioned in Section 2, in a bijel membrane reactor three or four regions depending on the presence or absence of the membrane support can be considered. It can be shown that the concentration of different species on the boundaries of these regions can be related to each other by a partition coefficient. The following equation describes the equilibrium between two adjacent regions in a bijel membrane reactor:

$$c_i^{\alpha} = \mathcal{K}_i^{\alpha,\beta} c_i^{\beta}, \tag{18}$$

where $\mathcal{K}_i^{\alpha,\beta}$ is the partition coefficient between α and β regions, α denotes the lumen or shell region, β represents the bijel region, and c_i^{α} and c_i^{β} denote the concentrations of component i on the α and β sides of the interface. The partition coefficient can be estimated as the fraction of aqueous or oily domains at the bijel surface. These fractions are determined from a phase diagram that has critical points in different locations, which depend on the desired composition (water/oil ratio). The bijel side of the interfaces between the bijel and the shell side and between the bijel and the lumen side can be divided into oily and aqueous domains. Thus, the partition coefficient can be estimated as the ratio of aqueous/oily domain area to the total surface area. We call the ratio of the surface area that is covered by the oily (or aqueous) phase to the total surface area of the bijel interface as the bijel surface oily (or aqueous) domain fraction.

2.5 | Boundary conditions

Equations (4)–(7) and (14)–(17) are the model equations that need to be solved using appropriate boundary conditions. As mentioned in Section 2.2, the bijel can be viewed as a porous medium with respect

to each phase. The main challenge is that there are two distinct regions on the boundary of a porous media with a continuous region. One region is saturated with the liquid phase, and in this region, velocity and surface tension continuities hold. However, the other region is the porous matrix, and in this region the no-slip condition holds. Empirical boundary conditions have been proposed to handle these challenges.[31]

In the current work, for the interface between the bijel and the continuous phase, the continuity of the tangential component of stress on the boundaries is assumed to hold. Additionally, it is assumed that the inlet mass flow rate, mass fractions of components, and the outlet pressure of shell and lumen flows are known. For the concentration boundary conditions, mass conservation equations on interfaces have been used. Table 1 summarizes all boundary conditions, where subscripts *in* and *out* denote the inlet and outlet conditions, and superscripts α and β represent the two sides of the interface.

It should be noted that at the interface of the bijel and the shell side, there are two types of interfaces; that is, the oil–aqueous and oil–oil interfaces (Figure 2). At the oil–aqueous interfaces, we assume the continuity of tangential and normal stresses. The continuity of tangential stress supports the continuous removal of the immiscible phase, which is coming from the bijel layer into the shell or lumen side. By approximating the capillary pressure equal to zero, which is a reasonable approximation (because of the continuous removal of the immiscible phase), the continuity of normal stresses results in the equality of pressure at the interface. Thus, in the cases where there is a pressure difference between the lumen and shell sides, a continuous radial flow through the bijel membrane is possible. However, this is not the regime in which bijel reactive separation should be run in.

3 | NUMERICAL SOLUTION APPROACH

To solve the model equations with the boundary conditions in Table 1, we apply the control volume method described in reference 37. To achieve this, the space is discretized as shown in Figure 3. φ and $\bar{\varphi}$ represent a field variable (e.g., concentration, velocity, etc.) inside and on the boundaries of the cells, respectively. Here, $j = 1,\ldots,N_z$ and $k = 1,\ldots,N_r$, where N_z and N_r are the number of cells in the z and r directions, respectively. Figure 4 shows the discretization approach in the cylindrical coordinates.

Based on the regions defined in Section 2, the discretized equations are presented in the next sections.

TABLE 1 Boundary conditions.

Position	Momentum equation	Mass conservation
Shell and lumen side flows at inlet	$v_z = v_{in}$ $v_r = 0$	$c_i = c_{iin}$
Shell and tube side flows at outlet	$P = P_{out}$	
Lumen side flow at the center	$v_r = 0$ $\frac{\partial v_z}{\partial r} = 0$	$\frac{\partial c_i}{\partial r} = 0$
Shell side flow at the wall	$v_r = 0$ $v_z = 0$	$\frac{\partial c_i}{\partial r} = 0$ $\frac{\partial c_i}{\partial z} = 0$
Interfaces between bijel and shell or lumen side flows	$P^i = P$ $v_r = u_r$	$c_i^\alpha = \mathcal{K}_i^{\alpha,\beta} c_i^\beta$ $v_r c_i^\alpha - D_i^\alpha \frac{\partial c_i^\alpha}{\partial r} = u_r^\beta c_i^\beta - D_i^\beta \frac{\partial c_i^\beta}{\partial r}$

3.1 | Shell and lumen regions

As mentioned in Section 2.1, Equations (5)–(8) describe the system in these regions. Using the boundary conditions in Table 1, for the shell side, Equations (5) and (7) can be solved analytically as follows:

$$v_z = \frac{1}{4\mu}\frac{dP}{dz}\left(r^2 - R^2\right), \tag{19}$$

$$v_r = \frac{1}{16\mu}\frac{d^2P}{dz^2}\left(2R^2 r - r^3\right), \tag{20}$$

where R is the radius of the shell.

For the lumen side, one can write:

$$v_z = \frac{1}{4\mu}\frac{dP}{dz}\left(r^2 - R_0^2\right), \tag{21}$$

$$v_r = \frac{1}{16\mu}\frac{d^2P}{dz^2}\left(2R_0^2 r - r^3\right) + \frac{R_0}{r}\left(u_r - \frac{1}{16\mu}\frac{d^2P}{dz^2}R^3\right), \tag{22}$$

where R_0 is the lumen radius, and $u_r = L_p \Delta P_r$. ΔP_r is the transmembrane pressure drop, and L_p is the hydraulic permeability:

$$L_p = \frac{K^l}{\mu^l \Delta R}.$$

Here, ΔR is the membrane thickness. Noting Equations (19)–(22), the velocity terms inside the region can be calculated. A finite volume form of Equation (7) for the jkth cell (Figure 4) is:

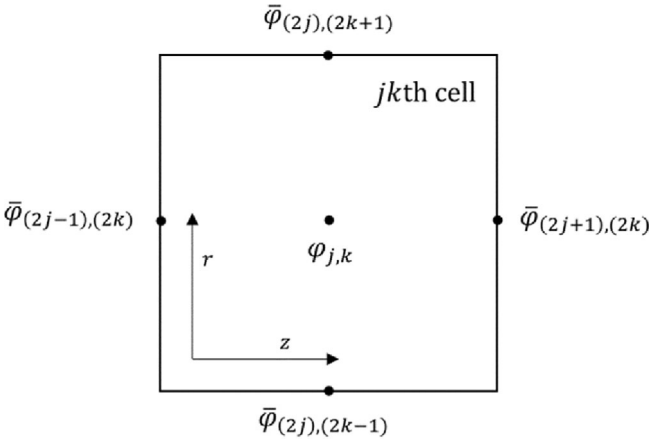

FIGURE 3 Planar representation of the spatial discretization in this work; the jkth cell.

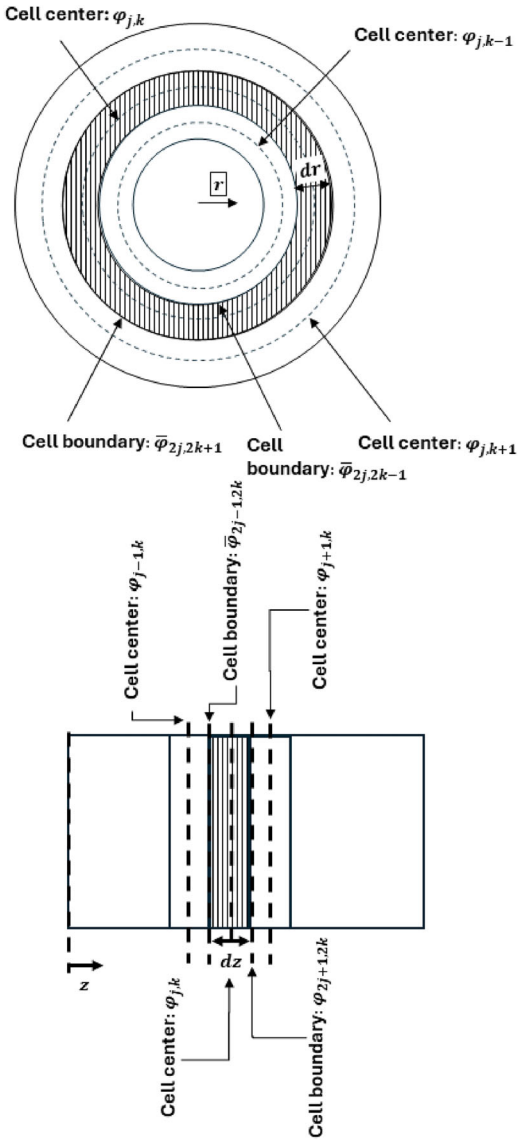

FIGURE 4 Cylindrical representation of the spatial discretization in this work (top: the radial view; bottom: the axial view).

$$\frac{(\bar{c}_i\bar{v}_z)_{2j-1,2k}-(\bar{c}_i\bar{v}_z)_{2j+1,2k}}{\Delta z}\frac{\Delta(r^2)}{2}+D_i r_{2k-1}\frac{(c_i)_{j,k}-(c_i)_{j,k-1}}{\Delta r}-D_i r_{2k+1}\frac{(c_i)_{j,k+1}-(c_i)_{j,k}}{\Delta r}=0, \tag{23}$$

where Δr and Δz are the control volume (cell) dimensions. We use the upwind scheme proposed in reference 37 to describe the concentration of component i on the boundary of two adjacent cells:

$$(\bar{c}_i)_{(2j+1),(2k)}=\begin{cases}(c_i)_{j,k}, & v_z>0\\ (c_i)_{j+1,k}, & v_z<0\end{cases}, \tag{24}$$

Since the accuracy of the upwind scheme is low, a small discretization interval size should be used. To address this issue, the exact (analytical) solution in the z direction obtained for the case of no diffusion is used to obtain an estimate of the functional form of the dependence of $(c_i)_{2j+1,2k}$ on $(c_i)_{j,k}$ and $(c_i)_{j+1,k}$:

$$\frac{\partial(v_z c_i)}{\partial z}=0\Rightarrow$$

$$(\bar{v}_z\bar{c}_i)_{2j+1,2k}=\frac{(v_z c_i)_{j+1,k}-(v_z c_i)_{j,k}}{\Delta z}(z_{2j+1}-z_j)+(v_z c_i)_{j,k}. \tag{25}$$

Using Equations (19)–(25), Equation (7) for the lumen and shell regions' cells takes the following linear form:

$$a_{j,k}(c_i)_{j,k}=a_{j+1,k}(c_i)_{j+1,k}+a_{j-1,k}(c_i)_{j-1,k}+a_{j,k+1}(c_i)_{j,k+1}+a_{j,k-1}(c_i)_{j,k-1}+b, \tag{26}$$

where $a_{M,N}, a_{M+1,N}, a_{M-1,N}$, $a_{M,N+1}$, and b are positive constants.

3.2 | Bijel and support layer regions

Because of the low axial pressure drop and the high momentum loss in the bijel (membrane matrix) due to flow in intertwined channels, the axial velocity can be neglected in this region. Thus, one can write:

$$u_r=L_p\Delta P_r, \tag{27}$$

$$u_z=0. \tag{28}$$

The basic idea behind the developed model in Section 2.2 is that each phase is continuous. Without the loss of generality, we consider Equation (16) for the aqueous phase. By integrating Equation (16) over the control volume (Figure 4), one can write:

$$\left(-D_i\frac{(c_i)_{j,k}-(c_i)_{j-1,k}}{\Delta z}+D_i\frac{(c_i)_{j+1,k}-(c_i)_{j,k}}{\Delta z}\right)\frac{\Delta(r^2)}{2}+\left(-D_i r_{2k-1}\frac{(c_i)_{j,k}-(c_i)_{j,k-1}}{\Delta r}+(r\bar{u}_r\bar{c}_i)_{2j,2k-1}\right)\Delta z-\left(-D_i r_{2k+1}\frac{(c_i)_{j,k+1}-(c_i)_{j,k}}{\Delta r}+(r\bar{u}_r\bar{c}_i)_{2j,2k+1}\right)\Delta z+\mathcal{R}_i\frac{\Delta(r^2)}{2}\Delta z=0, \tag{29}$$

The problem with Equation (29) is that the general form of the reaction term, $\mathcal{R}_i$, is nonlinear. As proposed in reference 37, this term should be linearized as follows:

$$\mathcal{R}_i=\mathcal{R}_i^*+\left(\frac{\partial\mathcal{R}_i}{\partial c_i}\right)^*(c_i-c_i^*), \tag{30}$$

where c_i^* is the value of c_i in the previous step of calculation, and superscript $*$ on a term indicates that the term is calculated based on c_i^*. As mentioned in Section 3.1, the values of c_i between nodes (boundary nodes) should be defined. We can use the upwind

approach, or we can develop an equation for c_i, if higher accuracy is desired. Using a similar approach as in Equation (25), for the r direction, one can write:

$$\frac{D_i}{r}\frac{\partial}{\partial r}\left(\frac{ru_r}{D_i}c_i - r\frac{\partial c_i}{\partial r}\right) = 0. \tag{31}$$

Let $Pe_r = \frac{ru_r}{D_i}$ which Pe_r is the Peclet number in the r direction. Based on the solution of Equation (31) ($c_i \propto r^{Pe_r}$), one can write:

$$(\bar{c}_i)_{2k-1} = \frac{r_{2k-1}^{Pe_r} - r_{k-1}^{Pe_r}}{r_{2k-1}^{Pe_r} - r_k^{Pe_r}}\left((c_i)_{j,k-1} - (c_i)_{j,k}\right) + (c_i)_{j,k-1}. \tag{32}$$

By using the upwind approach or Equation (32) and the linearization reaction term in (30), Equation (29) can be written in the form of Equation (26). This discretization converts the bijel membrane reactor equations into a set of linear equations in the form of (26), which can be solved iteratively.

4 | CASE STUDY

An experimental study by Cha et al.[13] showed that bijels can accelerate enzymatic reactions and can enable continuous reactive separations in enzymatic membrane reactors. Although this investigation showed promising results, there is very little experimental data from enzymatic bijel membrane reactors for model validation. The model developed in this work assumed that the oily and aqueous phases flow in channels separated by nanoparticles in the bijel; that is, there is no direct contact between the two phases. However, in a conventional biphasic membrane reactor, the void volume is occupied by both immiscible phases, and there is a two-phase flow in the membrane, the modeling of which requires considering saturation and capillary pressure.[23] Conversely, if the membrane matrix is highly hydrophobic or highly hydrophilic, then the void volume of the membrane is dominated by one phase, and thus, our model can predict the membrane behavior satisfactorily (especially when diffusion is dominant).

To validate our model, we consider the conventional biphasic membrane reactor containing immobilized β-glucosidase for the hydrolysis of oleuropein studied in reference 4, in which the effect of transmembrane flow velocity on the transmembrane reactor conversion was investigated experimentally. We evaluate the accuracy of our model predictions by comparing the model predictions with the experimental results reported in reference 4. Nagy et al.[9] studied mathematical modeling of this same membrane reactor. However, as they did not consider product inhibition in their model, and their model is lumped, their model predictions are not accurate at high residence times. Furthermore, although their model predicts the trend of transmembrane conversion versus transmembrane velocity, their model cannot predict that the conversion reaches a plateau as the transmembrane velocity decreased. Herein, we account for spatial concentration distributions and product inhibition in the model, improving the accuracy of the model especially at high residence times.

Mazzei et al.'s experimentally studied the hydrolysis of oleuropein using immobilized β-glucosidase as the enzyme.[4] Figure 5 depicts a schematic of their membrane structure. Inside the membrane, the following enzymatic reaction occurs:

$$\text{Oleuropein} + \text{Water} \rightarrow \text{Algycon} + \text{Glucose}, \tag{33}$$

which is described by the Michaelis–Menten model of Equation (17). In reference 4, oleuropein was fed to the membrane module in the shell side as the substrate, and the hydrophobic product, Algycon, was extracted by an organic phase flowing in the lumen side. The reaction took place inside the membrane sponge matrix in which the enzyme was immobilized on it. The local transmembrane conversion is defined by:

$$\text{Conversion} = \frac{C_i(r_e,z) - C_i(r_0,z)}{C_i(r_e,z)}, \tag{34}$$

where C_i denotes the reactant concentration.

As the axial pressure drop in a membrane reactor is small[30] and the momentum loss in the membrane matrix is negligible, the axial velocity in Equation (16) can be ignored. Furthermore, based on Equation (14), the transmembrane velocity (U_r) is proportional to the transmembrane pressure drop. Assuming small pressure drops in the axial direction implies that U_r is constant in the axial direction. Consequently, Equations (14)–(16) can be used to describe the membrane region.

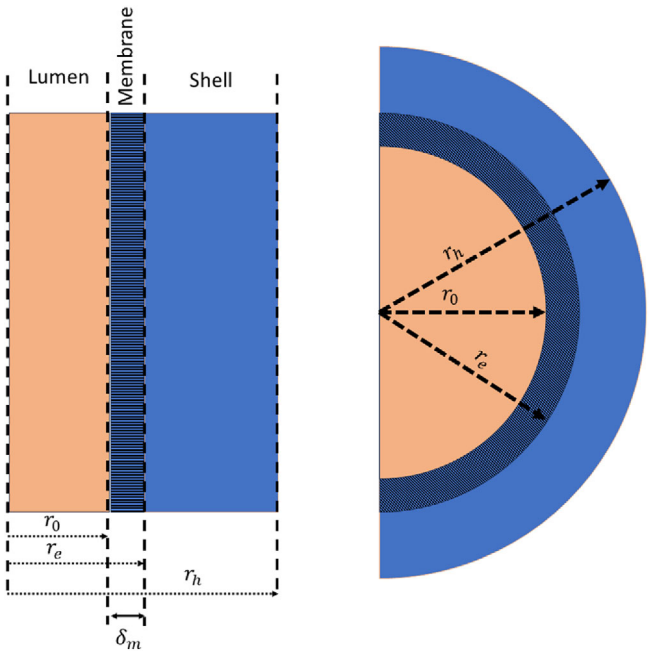

FIGURE 5 Schematic of the membrane reactor used in reference 4.

The membrane module contains four hollow fiber membranes with a total void volume of 0.54 cm^3. The external and internal diameters of the hollow fiber membranes are 1.08×10^{-3} m and 1.75×10^{-3} m. Thus, the membrane matrix thickness is 3.55×10^{-4} m. In reference 4, a value for the pitch between hollow fibers has not been reported and as a result, we consider the shell diameter as an unknown model parameter, which will be estimated from the reported measurements. The substrate-containing phase enters the shell side with an axial velocity of 0.35 m/s and the inlet concentration of oleuropein is 2.5 mol/m^3. An oily phase named limonene is passed through the lumen side with an axial velocity of 0.01 m/s. In reference 5, based on a comprehensive experimental kinetics study, the following Michaelis–Menten model parameter values have been reported: $\mathcal{R}_m = 9.7 \times 10^{-2}$ $mol/(m^3\,s)$ and $k_m = 3.8$ mol/m^3. A value of 0.019 mol/m^3 estimated from the experimental data reported in reference 4 has been reported for k_l in reference 9. Also, the value of the diffusion coefficient of the substrate has been calculated in reference 9 as 3.7×10^{-10} m^2/s using the Stokes-Einstein equation. The partition coefficient can be estimated as the fraction of oily and aqueous domains on the surface of the membrane.

4.1 | Model validation

The model equations are solved using the solution strategy described in Section 3. We consider 40 nodes in z direction and 30 nodes for each region in r direction (90 nodes in total for the z direction) to discretize the equations. We also increase the number of nodes to 60 and 90 for z and r directions, respectively, to evaluate the dependency of the numerical results on the mesh size.

Mazzei et al.[4] studied the effect of transmembrane pressure drop on the conversion. They defined the transmembrane resident time based on the volume of the membrane reactor and permeate flow rate to explain the effect of transmembrane pressure drop. They performed experimental studies at 0.007, 0.006, 0.005, 0.004, 0.003, and 0.0011 cm^3/s permeate flow rates that are equivalent to 75, 90, 116, 140, 180, and 426 s resident times. Based on the reported total void volume of the membrane module, 0.54 cm^3, the porosity of each hollow fiber is $\varepsilon = 0.86$. Using these values, one can calculate the transmembrane velocities at r_o: 7.7, 6.6, 5.5, 4.3, 3.2, and 1.1×10^{-6} m/s, respectively, where r_0 is the membrane lumen radius. As mentioned earlier, the values of partition coefficients are considered as the pore fraction on the surfaces of the membrane, that is, $K = 0.86$.

Because the shell diameter has not been reported in reference 4, we considered it as an adjustable (unknown) parameter to be estimated. The best results were obtained for the shell diameter equal to 1.00×10^{-4} m. Using the reported maximum value of reaction rate for the membrane reactor in reference 5, the presented model in current work predictions of the conversion did not agree with the measured conversions reported in reference 4. The same conversion versus resident time trend was observed, but conversion values were lower, which can be attributed to the difference between the immobilized enzyme concentration inside the membrane in references 5 and 4. As a result, we use the reported maximum value of reaction rate for the free enzyme case in reference 5 ($\mathcal{R}_m = 9.7$ $mmol/m^3\,s$). As mentioned earlier, because enzyme immobilization can enhance the enzyme activity,[2,7] this value for $\mathcal{R}_m$ is reasonable. Because of product removal in the membrane reactor during the reaction, it is expected that the product inhibition be lower for the membrane reactor in comparison to a stirred tank reactor. However, as mentioned earlier, it cannot be avoided completely. Thus, we consider the product inhibition coefficient as another unknown model parameter to be estimated. The estimation led to a value of 5 mol/m^3 for k_I, which is much higher than the calculated value for product inhibition for a stirred tank reactor (0.019 mol/m^3) reported in reference 9, but it shows that product inhibition should be considered in biphasic membrane reactors.

Figure 6 compares the model predicted and measured values of the average transmembrane conversion. This average conversion was obtained by calculating the mean of the local conversion, given by Equation (34), along the length. In this and next figures, we simply refer to this average conversion as transmembrane conversion. It shows that the model has good prediction accuracy, especially for high residence time. The model predicts that by increasing the residence time, reactant conversion in the membrane reactor increases until it reaches a maximum value. After that, any further increase in the residence time does not lead to any increase in the conversion. On the other hand, at low residence times, the model prediction accuracy is lower, which is not surprising. As we increase the transmembrane velocity (lowering the residence time), the convection mechanism inside the membrane becomes more important. However, to reduce the uncertainty and computational load of the model, we simplify the flow equation into Equation (27). Furthermore, the assumption behind Equations (9)–(11) is that two phases are co-continuous. While, as the transmembrane velocity is increased, one phase dominates the membrane region. Thus, the prediction accuracy of the model for membrane reactors decreases with increased transmembrane velocity. As membrane reactors usually work at high conversions, this model can be used reliably in

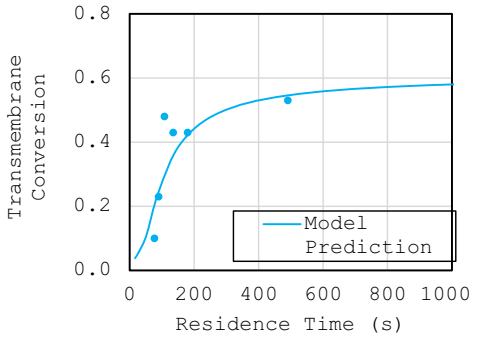

FIGURE 6 Conversion versus residence time in the membrane reactor. The data points represent the experimental measurements, and the solid line denotes the model prediction.

the design and optimization of membrane reactors at these conversions.

Note that in a bijel membrane reactor, the porous membrane acts just as a support for the bijel and contains only one phase, and the bijel has co-continuous conditions. Thus, the accuracy of this bijel membrane reactor model at high transmembrane velocities is expected to be satisfactory.

5 | RESULTS AND DISCUSSION

5.1 | Bijel versus conventional biphasic membrane reactor

In reference 9, a similar mathematical model to the one presented herein was used to describe a conventional membrane reactor with a biphasic reaction, and experimental data reported in reference 4 was used to validate the model. The model in reference 9 was developed for single-phase flow in a porous medium. As stated earlier, the model can predict with good accuracy, if the membrane is highly hydrophobic or hydrophilic. However, in a biphasic conventional membrane reactor the void volume is occupied by both aqueous and oily phases, necessitating a more complex model that accounts for saturation and capillary pressure concepts.[23] Thus, both the model presented herein and the model in reference 9 should be able to predict the experimental results in reference 4 adequately well.

In their modeling of a biphasic membrane reactor, Nagy et al.[9] assumed that the product inhibition does not occur (i.e., $k_I = \infty$), which led to the poor accuracy of their model at high residence times. In a biphasic membrane reactor, there is no flow within the membrane, and thus the oily product of the reaction is not removed from the reaction sites instantaneously, leading to production inhibition. In our work, k_I was estimated to be $5\,\mathrm{mol/m^3}$.

In the case of the bijel membrane reactor considered in this work, the reaction occurs on the surface of nanoparticles on which an enzyme is immobilized. The nanoparticles separate the oily phase from the aqueous phase. The mass transfer between the two phases occurs through the tiny pores between the nanoparticles, which in general may limit the separation rate. We assume that the size of the product molecules to be smaller than the space between nanoparticles, allowing for easy transport of the product to the oily phases and instantaneous removal of the product from the reaction sites. Because of the high specific surface area of nanoparticles at the interface, the enzyme concentration is likely to be higher in a bijel in comparison to a membrane matrix. Unlike in a biphasic membrane reactor in which only a fraction of the membrane thickness should be considered as a reacting medium, in a bijel reactor the reactant can penetrate the entire thickness of the membrane homogeneously, and thus the whole thickness of the medium is available for the reaction.

We use the model to compare reactant conversion in a bijel membrane reactor with that of the conventional membrane reactor simulated in Section 4.1. We assume that in the bijel membrane reactor, product inhibition does not occur. All the other parameters, including dimensions, residence times, kinetics parameters, partition coefficients, and operational conditions are the same. Figure 7 depicts the results. The model predicts that conversion in the bijel membrane reactor is higher than that in the membrane reactor, which is in agreement with the experimental results reported in reference 28. It should be noted that we considered only the effect of product inhibition. Based on the results of the simulation, the bijel can increase reactant conversion in conventional membrane reactors by about 20%, which is of importance in terms of process intensification.

Figure 7 indicates that as the pressure difference across the membranes decreases (as the residence time increases), the transmembrane conversion increases. Note that high pressure drops result in the impurity of the immiscible phase in the lumen or shell side (based on the direction of the pressure drop), which may not be desirable.

5.2 | Bijel membrane reactor analyses

5.2.1 | Effect of design specifications

Based on the simulation results presented in Figure 7, the transmembrane conversion in a bijel membrane reactor depends on the transmembrane velocity (transmembrane resident time). As the maximum conversion occurs at low transmembrane velocities, we consider the transmembrane velocity at r_0 to be $1.0 \times 10^{-7}\,\mathrm{m/s}$ and study the effect of design parameters on the maximum conversion in the bijel membrane reactor.

Based on references 18, 19, the internal microstructure of the bijel can be tuned during manufacturing, leading to different macroscopic properties such as permeability, tortuosity, and surface area. Better understanding of the dependence of these properties on the internal microstructure of the bijel requires experimental and/or microscopic modeling that is out of the scope of the current study. However, in the "Interface of regions" section, we have proposed a model that can be used to study the macroscopic effects of a microstructure-related parameter on the performance of the reactor.

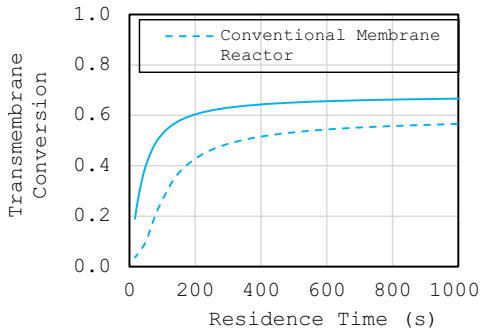

FIGURE 7 Comparison of the conversion in a bijel membrane reactor with that in a conventional membrane reactor.

5.2.2 | Effect of the bijel surface oily and aqueous domain fractions

Partition coefficients strongly affect the performance of bijel membrane reactors. As mentioned in Section 2.5, the aqueous and oily phase domain fractions on the surface of the bijel membrane dictate the equilibrium concentrations of species in the bijel region. We describe these equilibrium concentrations using Equation (18), where the equilibrium constants $K_i^{\alpha,\beta}$ are the aqueous and oily phase domain fractions. As the surface domain fractions of a bijel can be adjusted during the fabrication of the bijel,[13,16,19] it can be considered a process design parameter.

Here, we study the effect of the aqueous phase partition coefficient on the transmembrane conversion. To achieve this end, we vary the aqueous phase partition coefficient in the range of 0.2 – 0.9 (equivalent to 20% – 90% of the aqueous domain fraction). As Figure 8 shows, the transmembrane conversion is strongly affected by the reactant-side (aqueous phase in this case) partition coefficient. At low partition coefficients, which is equivalent to low aqueous domain fractions on the shell surface, the concentration of reactant is low at the boundary. Because the mass transfer inside a bijel is mainly via diffusion, the reactant concentration is low in the whole domain of the bijel, which leads to low reaction rates. As the aqueous domain fraction increases, the reactant concentration increases in the bijel, which results in a higher reaction rate and transmembrane conversion. This indicates that the surface domain fractions of a bijel should be tuned during the fabrication process based on the reactions that will occur in the bijel membrane. This indicates that the surface domain fractions of a bijel should be tuned during the fabrication process based on the reactions that will occur in the bijel membrane.

5.2.3 | Effect of bijel thickness

We study the effect bijel thickness on the transmembrane conversion over a bijel thickness range of 8.4×10^{-5} m to 6.7×10^{-4} m. The lumen diameter is considered to be 1.08×10^{-3} m. As Figure 9 shows, the transmembrane conversion increases as the bijel thickness increases in a limited range of relative thickness, which is not surprising. By increasing the thickness, the volume of the reacting region increases, and therefore the conversion increases. The conversion plateau at high bijel thicknesses can be explained based on the available surface area on the shell side. By increasing the thickness of bijel, the shell surface area to reactor volume ratio decreases. As a result, by increasing the membrane thickness, the reactant flow to reactor volume ratio decreases, and the rate of increase in transmembrane conversion decreases. Thus, the bijel membrane thickness can be considered as a design parameter for optimization purposes.

5.2.4 | Effect of the lumen diameter

We study the effect of the lumen diameter on the transmembrane conversion over a lumen diameter range of 1.35×10^{-4} m to 2.70×10^{-3} m. The bijel membrane thickness is considered to be 3.35×10^{-4} m. Figure 10 shows that by increasing the lumen radius in a wide range, the transmembrane conversion increases. Because the bijel thickness is constant, by increasing the lumen radius the volume

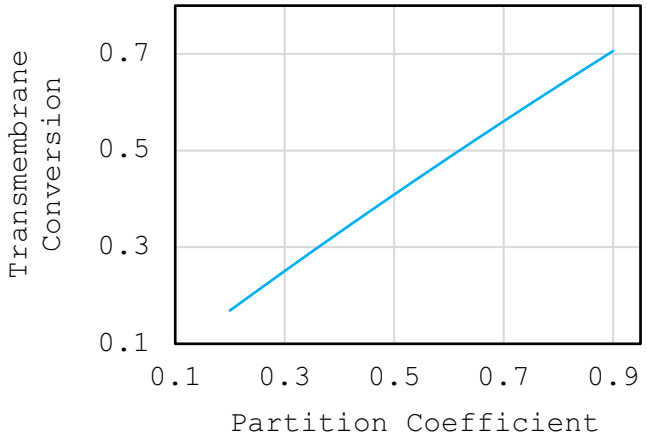

FIGURE 8 Effect of the aqueous phase partition coefficient on the transmembrane conversion.

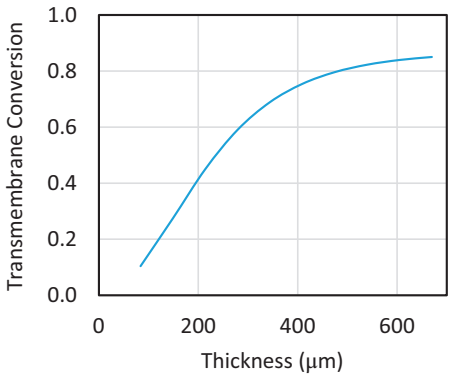

FIGURE 9 Effect of bijel thickness on the transmembrane conversion.

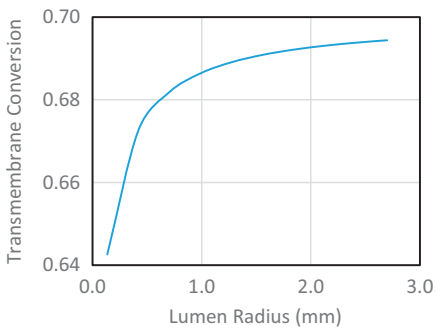

FIGURE 10 Effect of the lumen radius on the transmembrane conversion.

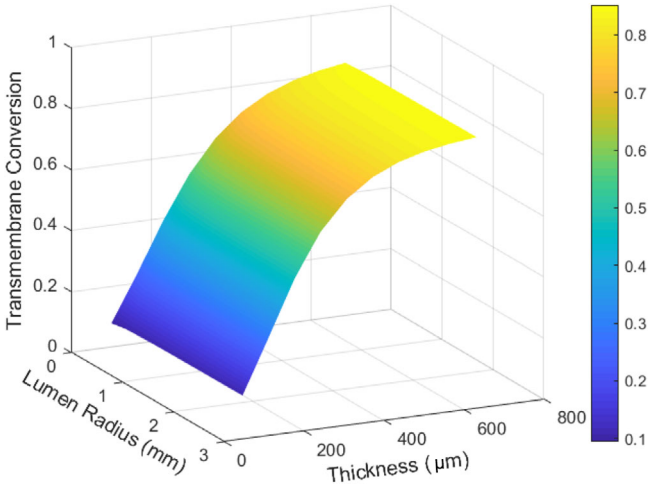

FIGURE 11 3D view of the effect of the lumen radius and the bijel thickness on the.

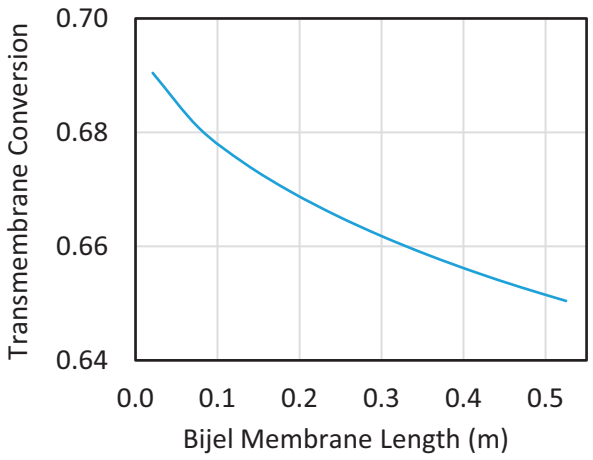

FIGURE 12 Effect of bijel membrane reactor length on the transmembrane conversion.

of the reacting region increases. As a result, the transmembrane conversion increases. The lower increase of conversion with increased lumen radius at high lumen radiuses is due to the fact that at high volumes, the reactant flow to reactor volume ratio is low, and thus, the conversion increases less with increased lumen radius. This study indicates that the lumen radius can also be considered as a design parameter for bijel membrane reactors.

As Figures 9 and 10 show, the performance of the bijel membrane reactor is affected by both the lumen radius and the bijel thickness. Figure 11 is a 3D graph that depicts how these important variables affect the performance of the bijel reactor. As seen in this figure, the bijel thickness has a stronger effect on the bijel reactor performance than the lumen radius. This implies that the lumen radius should be set based on the feasibility of the bijel manufacturing process, and the bijel thickness should be considered as a decision variable to achieve desirable performance.

5.2.5 | Effect of reactor length

We study the effect of the reactor length on the transmembrane conversion over a reactor length range of 2.1×10^{-2} m to 5.25×10^{-1} m. Figure 12 shows that the transmembrane conversion does not change substantially over the reactor length range. By increasing the reactor length, the concentration of the reactant at the end of the reactor decreases. As a result, at the end section of the bijel, there is a slight decrease in the reactant concentration (slight increase in the transmembrane conversion). It should be noted that a high axial velocity of 0.35 m/s was considered for the reactant flow on the shell side. Consequently, the reactant concentration does not change appreciably over the range of reactor length. If we decrease the axial velocity of the reactant, the effect of reactor length would be more significant.

5.2.6 | Effect of operation conditions

The transmembrane pressure drop, reactant inlet concentration, and shell side flow velocity are the operating conditions in the system. It should be noted that in an enzymatic reaction, pH and temperature are also important operational parameters. However, pH and temperature are usually kept constant using tight temperature and pH control. The effect of transmembrane pressure drop was studied in Section 5.1. Like in Section 5.2. we assume a transmembrane velocity at r_0 of 1.0×10^{-7} m/s in this section.

5.2.7 | Effect of reactant inlet concentration

We study the effect of the reactant inlet concentration over a concentration range of 0.25 to 25 $\mathrm{mol/m^3}$. As Figures 13 and 14 depict, by increasing the inlet concentration, the transmembrane conversion decreases, but the product concentration increases. Based on the Michaelis–Menten model, at low reactant concentrations, the reaction can be considered as a first-order reaction, but at high concentrations, the order is zero. Thus, the reactant inlet concentration is an effective operating parameter to optimize the reactor performance.

5.2.8 | Effect of shell-side flow axial velocity

The effect of the shell-side flow axial velocity on the transmembrane conversion is studied by over the axial velocity range of 0.035 – 1.75 m/s. Figure 15 shows that the shell-side axial velocity has a negligible effect on the transmembrane conversion, which is not surprising. The main mechanism for the mass transfer from the shell-side flow to the bijel is diffusion. For low axial velocities,

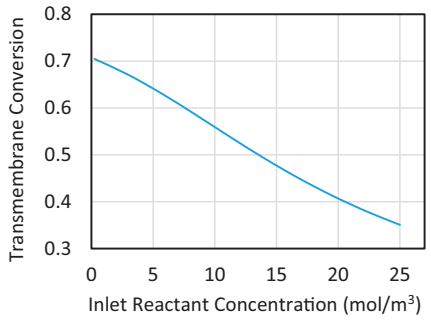

FIGURE 13 Effect of the inlet reactant concentration on the transmembrane conversion.

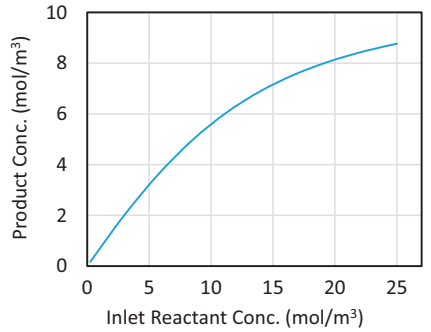

FIGURE 14 Effect of the inlet reactant concentration on the product concentration.

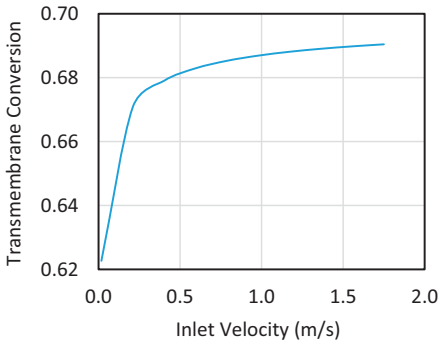

FIGURE 15 Effect of shell-side axial velocity on the transmembrane conversion.

because of higher axial residence time, the concentration of reactant is lower near the outlet. As a result, the transmembrane conversion in the bijel near the end of the reactor decreases very slightly. Thus, the shell-side flow axial velocity is not a good optimization parameter.

Both the reactor length and the axial velocity in the shell side strongly affect the residence time of the shell-side stream, as the transmembrane conversion was obtained by averaging the local transmembrane conversion. The 3D plot in Figure 16 shows how these variables affect the transmembrane conversion. Equation (18) describes the dependence of the concentration of the reactant on the outer surface of the bijel on the concentration of the reactant

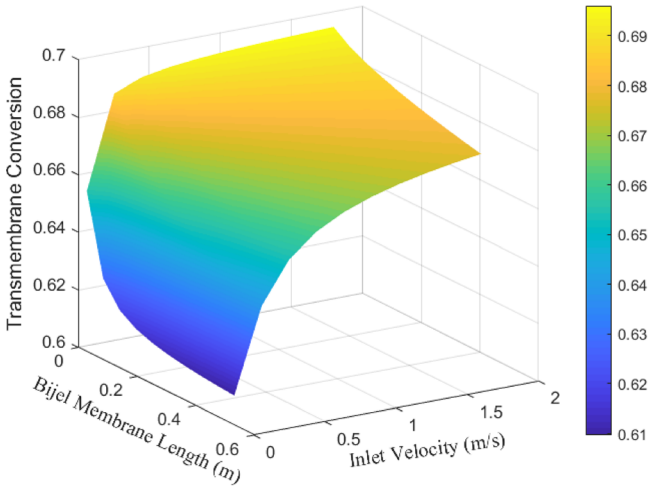

FIGURE 16 3D view of the effect of the axial velocity in the shell side and the reactor length on the transmembrane conversion.

in the shell side. By decreasing the shell-side velocity or increasing the length of the reactor, the shell-side reactant concentration near the outlet of the reactor decreases. As a result, based on Equation (18), the reactant concentration decreases in the bijel medium at the end of the reactor, and based on Equation (17) the reaction rate decreases. Consequently, there is a decrease in the transmembrane conversion.

6 | SUMMARY AND CONCLUSIONS

This study provided a mathematical framework for the development of process models for bijel membrane reactors. An efficient numerical solution strategy to solve the model equations was proposed. The case study showed that the developed model can predict the behavior of a real biphasic membrane reactor accurately. It was assumed that phases are co-continuous in the membrane region, which is a valid assumption, given the bijel structure. The simulation results show how the process design and operation parameters of a bijel membrane reactor should be adjusted to improve the performance of the reactor. The simulation study showed the strong effects of the aqueous and oily phase bijel surface domain fractions on the performance of the bijel reactor. This points to the importance of tuning these properties during bijel manufacturing. As the bijel membrane reactor technology is in its infancy, developing a mathematical model and providing a suitable solution method for solving the model equations are timely. The developed mathematical framework has applications in the scale-up, design, optimization, and control of bijel membrane reactors.

AUTHOR CONTRIBUTIONS

Aref Ghoreishee: Writing – original draft; validation; investigation. **Daeyeon Lee:** Conceptualization; funding acquisition; writing – review and editing. **Dimitrios Papavassiliou:** Conceptualization; writing – review

and editing; funding acquisition. **Kathleen Stebe:** Funding acquisition; conceptualization; writing – review and editing. **Masoud Soroush:** Supervision; funding acquisition; writing – review and editing; conceptualization.

ACKNOWLEDGMENTS

The authors would like to acknowledge financial support from the U.S. National Science Foundation under Grant No. CBET-2132141. Any opinions, findings, and conclusions or recommendations expressed in this material are those of the authors and do not necessarily reflect the views of the National Science Foundation.

DATA AVAILABILITY STATEMENT

This manuscript includes only numerical simulation data that were generated by solving the governing equations presented in the main body of this manuscript. The data that were used to generate the plots in Figures 6–12 are tabulated/available in Excel files in the Supplementary Materials (Data S1).

ORCID

Daeyeon Lee https://orcid.org/0000-0001-6679-290X
Dimitrios Papavassiliou https://orcid.org/0000-0002-4583-0820
Masoud Soroush https://orcid.org/0000-0002-4879-5098

REFERENCES

1. Drioli E, Brunetti A, Di Profio G, Barbieri G. Process intensification strategies and membrane engineering. *Green Chem*. 2012;14(6):1561-1572.
2. Mazzei R, Chakraborty S, Drioli E, Giorno L. Membrane bioreactors in functional food ingredients production. *Membrane Technology. Membranes for Food Applications*. Vol 3. Wiley; 2010:201-222.
3. Hu Y, Wang Y, Luo G, Dai Y. Modeling of a biphasic membrane reactor catalyzed by lipase immobilized in a hydrophilic/hydrophobic composite membrane. *J Membr Sci*. 2008;308(1–2):242-249.
4. Mazzei R, Drioli E, Giorno L. Enzyme membrane reactor with heterogenized β-glucosidase to obtain phytotherapic compound: optimization study. *J Membr Sci*. 2012;390:121-129.
5. Mazzei R, Giorno L, Piacentini E, Mazzuca S, Drioli E. Kinetic study of a biocatalytic membrane reactor containing immobilized β-glucosidase for the hydrolysis of oleuropein. *J Membr Sci*. 2009;339(1–2):215-223.
6. Andrić P, Meyer AS, Jensen PA, Dam-Johansen K. Reactor design for minimizing product inhibition during enzymatic lignocellulose hydrolysis: I. Significance and mechanism of cellobiose and glucose inhibition on cellulolytic enzymes. *Biotechnol Adv*. 2010;28(3):308-324.
7. Haupt B, Neumann T, Wittemann A, Ballauff M. Activity of enzymes immobilized in colloidal spherical polyelectrolyte brushes. *Biomacromolecules*. 2005;6(2):948-955.
8. Cook P, Gove F. Transcription by an immobilized RNA polymerase from bacteriophage T7 and the topolgy of transcription. *Nucleic Acids Res*. 1992;20(14):3591-3598.
9. Nagy E, Dudás J, Mazzei R, Drioli E, Giorno L. Description of the diffusive–convective mass transport in a hollow-fiber biphasic biocatalytic membrane reactor. *J Membr Sci*. 2015;482:144-157.
10. Giorno L, Molinari R, Natoli M, Drioli E. Hydrolysis and regioselective transesterification catalyzed by immobilized lipases in membrane bioreactors. *J Membr Sci*. 1997;125(1):177-187.
11. Prazeres D, Cabral J. Enzymatic membrane bioreactors and their applications. *Enzyme Microb Technol*. 1994;16(9):738-750.
12. Lozano P, Pérez-Marın A, De Diego T, et al. Active membranes coated with immobilized Candida Antarctica lipase B: preparation and application for continuous butyl butyrate synthesis in organic media. *J Membr Sci*. 2002;201(1–2):55-64.
13. Cha S, Lim HG, Haase MF, Stebe KJ, Jung GY, Lee D. Bicontinuous interfacially jammed emulsion gels (bijels) as media for enabling enzymatic reactive separation of a highly water insoluble substrate. *Sci Rep*. 2019;9(1):6363.
14. Di Vitantonio G, Lee D, Stebe KJ. Fabrication of solvent transfer-induced phase separation bijels with mixtures of hydrophilic and hydrophobic nanoparticles. *Soft Matter*. 2020;16(25):5848-5853.
15. Di Vitantonio G, Wang T, Haase MF, Stebe KJ, Lee D. Robust bijels for reactive separation via silica-reinforced nanoparticle layers. *ACS Nano*. 2018;13(1):26-31.
16. Di Vitantonio G, Wang T, Stebe KJ, Lee D. Fabrication and application of bicontinuous interfacially jammed emulsions gels. *Appl Phys Rev*. 2021;8(2):021323.
17. Haase MF, Stebe KJ, Lee D. Continuous fabrication of hierarchical and asymmetric bijel microparticles, fibers, and membranes by solvent transfer-induced phase separation (STRIPS). *Adv Mater*. 2015;27(44):7065-7071.
18. Haase MF, Sharifi-Mood N, Lee D, Stebe KJ. In situ mechanical testing of nanostructured bijel fibers. *ACS Nano*. 2016;10(6):6338-6344.
19. Haase MF, Jeon H, Hough N, Kim JH, Stebe KJ, Lee D. Multifunctional nanocomposite hollow fiber membranes by solvent transfer induced phase separation. *Nat Commun*. 2017;8(1):1234.
20. Nagy E. *Basic Equations of Mass Transport through a Membrane Layer*. Elsevier; 2018.
21. Seidel-Morgenstern A. *Membrane Reactors: Distributing Reactants to Improve Selectivity and Yield*. John Wiley & Sons; 2010.
22. Blunt MJ. *Multiphase Flow in Permeable Media: A Pore-Scale Perspective*. Cambridge University Press; 2017.
23. Feder J, Flekkøy EG, Hansen A. *Physics of Flow in Porous Media*. Cambridge University Press; 2022.
24. Hsu C-J. *Numerical Heat Transfer and Fluid Flow*. Taylor & Francis; 1981.
25. Tian D, Hao R, Zhang X, et al. Multi-compartmental MOF microreactors derived from Pickering double emulsions for chemo-enzymatic cascade catalysis. *Nat Commun*. 2023;14(1):3226.
26. Li K, Zou H, Ettelaie R, Zhang J, Yang H. Spatial localization of two enzymes at Pickering emulsion droplet interfaces for cascade reactions. *Angew Chem*. 2023;135(15):e202300794.
27. Zou H, Shi H, Hao S, Yang J, Tian X, Yang H. Boosting catalytic selectivity through a precise spatial control of catalysts at Pickering droplet interfaces. *J Am Chem Soc*. 2023;145(4):2511-2522.
28. Vitantonio GD. *Bijels for Continuous Reactive Separations* [Unpublished Doctoral Dissertation]. Publicly Accessible Penn Dissertations: 4457. University of Pennsylvania; 2021.
29. Bird RB. Transport phenomena. *Appl Mech Rev*. 2002;55(1):R1-R4.
30. Apelblat A, Katzir-Katchalsky A, Silberberg A. A mathematical analysis of capillary-tissue fluid exchange. *Biorheology*. 1974;11(1):1-49.
31. Nield DA, Bejan A. *Convection in Porous Media*. Vol 3. Springer; 2006.
32. Tsai SW, Wu GH, Chiang CL. Kinetics of enzymatic hydrolysis of olive oil in biphasic organic–aqueous systems. *Biotechnol Bioeng*. 1991;38(7):761-766.
33. Caminal G, Lopez-Santin J, Sola C. Kinetic modeling of the enzymatic hydrolysis of pretreated cellulose. *Biotechnol Bioeng*. 1985;27(9):1282-1290.
34. Al-Zuhair S. Kinetics of hydrolysis of tributyrin by lipase. *J Eng Sci Technol*. 2006;1:50-58.
35. McDevitt K, Thorson T, Botvinick E, Mumm D, Mohraz A. Microstructural characteristics of bijel-templated porous materials. *Materialia*. 2019;7:1003932019.

36. Reeves M, Stratford K, Thijssen JH. Quantitative morphological characterization of bicontinuous Pickering emulsions via interfacial curvatures. *Soft Matter*. 2016;12(18):4082-4092.
37. Patankar SV. *Numerical Heat Transfer and Fluid Flow*. CRC Press; 2018.

SUPPORTING INFORMATION

Additional supporting information can be found online in the Supporting Information section at the end of this article.

How to cite this article: Ghoreishee A, Lee D, Papavassiliou D, Stebe K, Soroush M. Modeling and simulation of bi-continuous jammed emulsion membrane reactors for enhanced biphasic enzymatic reactions. *AIChE J*. 2024; e18549. doi:10.1002/aic.18549